Holger Borchert*, Dorothea Scheunemann, Katja Frevert, Florian Witt, Andreas Klein, and Jürgen Parisi

Schottky Solar Cells with $CuInS_2$ Nanocrystals as Absorber Material

Abstract: Colloidal semiconductor nanocrystals with tunable optical properties are promising materials for light harvesting in solar cells. So far, in particular cadmium and lead chalcogenide nanocrystals were intensively studied in this respect, and the device performance has made rapid progress in recent years. In contrast, less research efforts were undertaken to develop solar cells based on Cd- and Pb-free nanoparticles as absorber material. In the present work, we report on Schottky solar cells with the absorber layer made of colloidal copper indium disulfide nanocrystals. Absorber films with up to ~ 500 nm thickness were realized by a solution-based layer-by-layer deposition technique. The device performance was systematically studied dependent on the absorber layer thickness. Decreasing photocurrent densities with increasing thickness revealed charge transport to be a limiting factor for the device performance.

Keywords: Schottky Solar Cells, Copper Indium Disulfide, Colloidal Nanocrystals, Layer-by-Layer Deposition.

DOI 10.1515/zpch-2014-0595
Received August 27, 2014; accepted October 9, 2014

Dedicated to Horst Weller on the occasion of his 60th birthday

***Corresponding author: Holger Borchert,** Carl von Ossietzky University of Oldenburg, Department of Physics, Energy and Semiconductor Research Laboratory, Carl-von-Ossietzky-Str. 9–11, 26129 Oldenburg, Germany, e-mail: holger.borchert@uni-oldenburg.de
Dorothea Scheunemann, Katja Frevert, Florian Witt, Jürgen Parisi: Carl von Ossietzky University of Oldenburg, Department of Physics, Energy and Semiconductor Research Laboratory, Carl-von-Ossietzky-Str. 9–11, 26129 Oldenburg, Germany
Andreas Klein: Technische Universität Darmstadt, Department of Materials and Geosciences, Surface Science Division, Jovanka-Bontschits-Straße 2, 64287 Darmstadt, Germany

1 Introduction

Many physical and chemical properties of crystallized matter can significantly change, when the size of the crystallites is reduced to a few nanometers. A prominent example is the quantum size effect, where reduction of the particle size below the Exciton Bohr radius causes a widening of the energy gap of inorganic semiconductors [1–3]. By consequence, optical properties such as the absorption edge and emission wavelength of semiconductor nanocrystals become tunable by controlling the particle size. The tunable optical properties together with the feature of solution-processability make colloidal semiconductor nanocrystals promising materials for the fabrication of optoelectronic devices such as light-emitting diodes [4, 5] or solar cells [6].

Different device concepts have been explored for solar cells with semiconductor nanoparticles in the absorber layer. Mainly, one can distinguish between hybrid solar cells where the inorganic nanoparticles are combined with conductive polymer [6–10], and devices where so-called quantum dot solids, i. e., compact layers of assembled nanoparticles alone, constitute the absorber layer [6, 11, 12]. In both cases, research has focused mainly on cadmium and lead chalcogenide nanocrystals as materials. Hybrid solar cells were reported to reach up to 4.7% power conversion efficiency (PCE) under standard test conditions with CdSe nanorods in combination with a low band gap polymer [13]. With alloys of PbS and PbSe, even 5.5% PCE were reached [14]. Devices with colloidal quantum dot solids can be constructed in different ways. In the simplest case, a nanoparticle layer with p-type conductivity is in contact with a low work function metal, forming a Schottky contact. Corresponding devices are called Schottky solar cells, and up to 4.6% have been reported for their power conversion efficiency, with PbSe used as absorber material [15]. In so-called depleted heterojunction solar cells, a p-type semiconductor nanoparticle layer is in contact with an n-type transition metal oxide, typically a porous titania layer. With this device concept, 8%–9% PCE were recently reported with colloidally prepared PbS quantum dots [16, 17].

Despite the remarkable progress made, the toxicity of the Cd- and Pb-based materials employed restricts the application potential. An alternative material could be $CuInS_2$ (copper indium disulfide, often abbreviated as CIS). Many procedures have been elaborated in recent years to synthesize structurally well-defined $CuInS_2$ nanocrystals by means of colloidal chemistry [18, 19]. In a preceding publication, we examined the applicability of colloidal $CuInS_2$ nanocrystals in solar cells using a heterojunction formed by layers of $CuInS_2$ and ZnO nanoparticles, respectively [20]. However, the device performance remained below 1% PCE. As one limiting reason, we found that the thickness of the $CuInS_2$ layer, which could be

reached in a single spin-coating step, was insufficient to harvest enough photons for high current densities [20].

In Pb-based solar cells with colloidal quantum dot solids, thicker absorber layers are usually prepared using layer-by-layer techniques [21–23]. Thereby, a thin layer is deposited from colloidal solution, and subsequently treated with cross-linking molecules which render the nanoparticle film insoluble in the solvent used in the colloidal solution. Therefore, another layer of nanoparticles can be deposited on top of the treated film. With several cycles of nanoparticle deposition and cross-linking treatments, absorber layers of several hundred nanometer thickness were reached with lead chalcogenide quantum dots [21, 22]. Apart from controlling the absorber layer thickness, layer-by-layer techniques allow for modification of the contact between individual nanocrystals in the films, because treatment with the cross-linking molecules leads to a partial exchange of organic ligands surrounding the colloidally prepared semiconductor nanoparticles. In the present work, we transferred such layer-by-layer methods to the $CuInS_2$ material system in order to build up nanoparticle layers with reasonable thickness in terms of sufficient light absorption. As-prepared nanoparticle absorber layers were tested with respect to their photovoltaic application in Schottky solar cells.

2 Experimental

Colloidal $CuInS_2$ nanocrystals were synthesized as described previously [20] using a rapid injection of a 1 : 1 mixture (by volume) of 1-dodecanethiol and tert-dodecanethiol into a reaction vessel containing copper acetate, indium(III) acetate, trioctylphosphine oxide and oleylamine at 220 °C. The mixture was then heated up to 250 °C, and the reaction was stopped after 1 h by cooling to room temperature. Afterwards, the particles were precipitated, washed with ethanol and redispersed in chlorobenzene in a concentration of 40–160 mg/mL.

Solar cells were prepared on cleaned indium tin oxide (ITO)-coated glass substrates covered with poly(3,4-ethylenedioxythiophene):poly(stryrene sulfonate) (PEDOT:PSS, Clevios P VP AI 4083). $CuInS_2$ films were prepared using a layer-by-layer spin-coating method with 3-mercaptopropionic acid as cross-linker, as adopted from procedures established for the preparation of quantum dot solids made of lead chalcogenide nanocrystals [22]. In an individual cycle of the layer-by-layer process, $CuInS_2$ nanocrystals were deposited via spin-coating in ambient atmosphere at 1250 rpm for 20 s. Subsequently, the films were treated with a solution of 3-mercaptopropionic acid in methanol (concentration: 10 vol. %), rinsed two times with pure methanol at 1250 rpm and heated for 10 min at 120 °C or

180 °C, respectively. These steps were repeated until the desired film thickness (measured using a Veeco Dektak 6M stylus profiler) was reached. Finally, top contacts (50 nm Mg followed by 120 nm Al) were thermally evaporated. Due to the limited charge carrier mobility of colloidal quantum dot solids, the active area of the solar cells was estimated as the geometric overlap of the electrodes, individually measured for each device, and was in the range of 0.12–0.14 cm^2.

The nanocrystals were structurally characterized using transmission electron microscopy (TEM, Zeiss EM 902 A), while $CuInS_2$ films were characterized using scanning electron microscopy (SEM, FEI Helios NanoLab 600i). X-ray photoelectron spectroscopy (XPS) measurements for interface analysis were performed using an ESCALAB 250 spectrometer, which is part of the Darmstadt Integrated System for Solar Cell Research (DAISY-SOL) [24]. The spectrometer is equipped with a monochromatic Al anode providing an excitation energy of 1486.6 eV. The measured binding energies are given with respect to the Fermi level, which is calibrated using sputter cleaned Ag and Cu samples. The (relative) uncertainty in the determination of the valence band maximum binding energy, which is determined by linear extrapolation of the leading edge of the valence band emission, is estimated to be 100 meV. Current density-voltage characteristics (J–V curves) of the photovoltaic devices were recorded using a Keithley 4200 semiconductor characterization system, while an AM1.5G solar simulator (Photo Emission Tech.) served as light source. The irradiance of the light field was adjusted to 100 mW/cm^2 using a calibrated silicon solar cell. Measurements of the external quantum efficiency (EQE) were performed without bias illumination on a Bentham PVE300 characterization system equipped with a lock-in amplifier (Stanford Research Systems SR830) operating at 230 Hz.

3 Results and discussion

The employed synthesis method yields colloidal $CuInS_2$ nanocrystals with a pyramid-like shape and spatial dimensions of the order of ~ 15 nm. Figure 1a shows a typical high-resolution TEM image of an individual nanocrystal. In this work, we investigated mercaptopropionic acid as a cross-linking molecule for preparing $CuInS_2$ nanoparticle films by layer-by-layer deposition. Figure 1b shows a typical SEM image of a $CuInS_2$ film on ITO after a single deposition and cross-linking cycle using an annealing temperature of 120 °C. As can be seen, a rather homogenous nanoparticle film was obtained. Figure 1c shows an image after applying 6 cycles. It is well visible that individual layers can be deposited on top of each other and that finally rather dense and homogeneous films are reached.

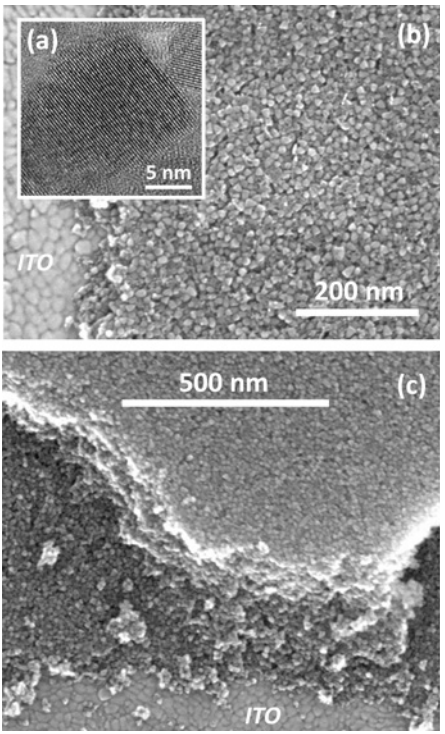

Figure 1: (a): High-resolution TEM image of the $CuInS_2$ nanocrystals. (b,c): SEM images of thin films obtained by layer-by-layer deposition after 1 cycle (b) and 6 cycles (c), respectively. After each cycle, the films were annealed at 120 °C. In both images, the nanoparticle film was removed at the border to visualize the underlying ITO substrate.

Figure 2 shows an analysis of the dependency of the nanoparticle layer thickness on the number of deposition cycles and the concentration of the colloidal solutions used for spin-coating. Within this work, layer thicknesses in the range of about 100–500 nm were reached. For the lower concentrations tested (40–80 mg/mL), the thickness increases as to be expected continuously with the number of deposition cycles, but interestingly, it appears nearly independent of the concentration. With the highest concentration investigated (160 mg/mL), the general trend of increasing thickness with increasing number of cycles is found as well, but the data scatter quite strongly, and repeating the manually handled procedure did not always yield the same thickness (see for example the two data points in Figure 2 obtained from independent samples with 5 deposition cycles and 160 mg/mL concentration).

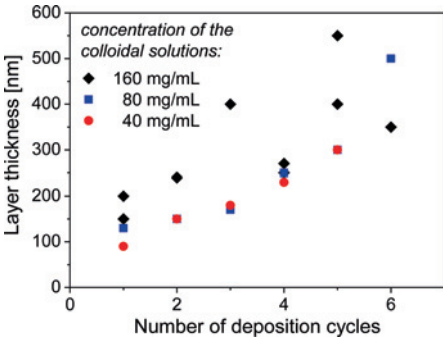

Figure 2: The thickness of the $CuInS_2$ nanoparticle layer as measured with a profilometer in dependence of the number of deposition cycles and the concentration of the colloidal solutions used for spin-coating. The annealing temperature was 120 °C. In some cases, several data points are shown for the same parameters. These correspond to independent samples and provide an impression of the reproducibility.

In conclusion from these experiments, the layer-by-layer deposition method using mercaptopropionic acid was successfully transferred from the lead chalcogenide systems to our material system, but the lower concentrations in the range of 40–80 mg/mL appear more favorable for a good control over the layer thickness. Furthermore, it should be mentioned that the number of cycles required to reach a certain thickness was significantly lower than reported in some works on Pb-based nanocrystals. For example, Szendrei et al. [23] reported a layer-by-layer deposition method for PbS quantum dots, where 1,4-benzenedithiol was used as cross-linker, and where the increase of the layer thickness in each cycle was only about 6–7 nm. Lowering the concentration of the solutions accompanied by increasing the number of cycles and automatization of the layer-by-layer procedure might be a way to improve the homogeneity of the $CuInS_2$ films and the degree of control over the final layer thickness in future.

In the next step, the realized $CuInS_2$ nanoparticle films were investigated with respect to their suitability as absorber layer in Schottky solar cells. Therefore, $CuInS_2$ films were prepared by the described layer-by-layer technique between ITO/PEDOT:PSS as anode and Mg/Al as cathode (see sketch in Figure 3a). Mg has a work function of 3.66 eV [25]. Values for the valence and conduction band edges of the $CuInS_2$ nanoparticles are available from an earlier study by cyclic voltammetry [26]. Therein, pyramidal-shaped $CuInS_2$ nanocrystals similarly prepared and then subjected to a surface treatment with pyridine were investigated, and the valence and conduction band edges were found to be located at -4.7 eV and -3.3 eV with respect to vacuum, respectively [26]. The position of the Fermi level of the $CuInS_2$ nanoparticles can be estimated from an investigation by photoelec-

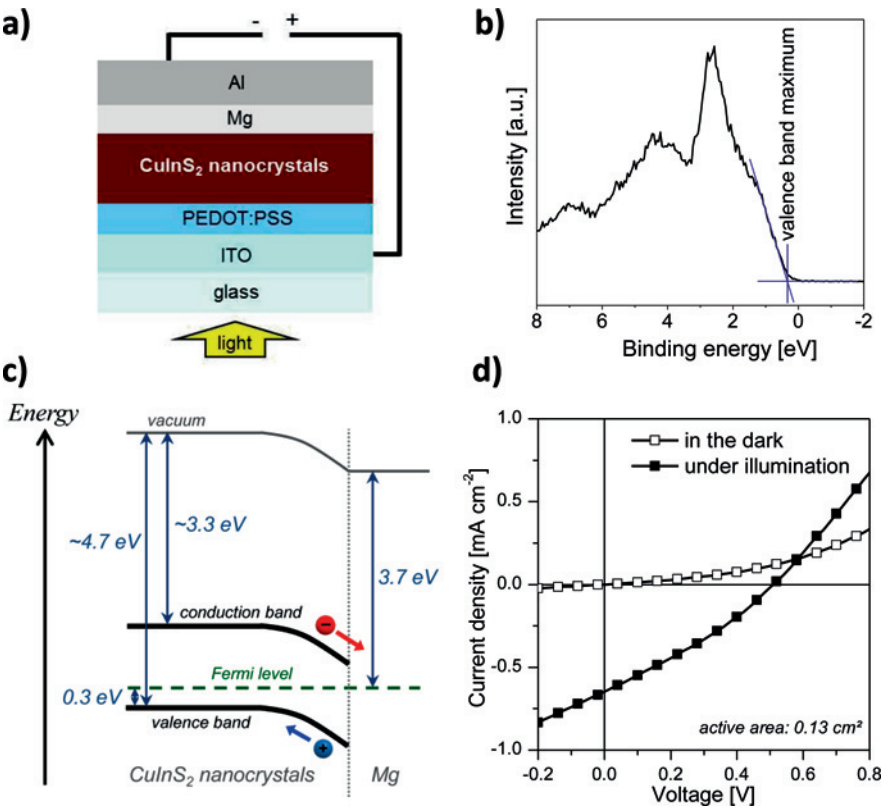

Figure 3: (a): Schematic sketch of the device architecture used. (b) Valence band spectrum for a $CuInS_2$ nanoparticle film on glass. The valence band maximum is located $\sim 0.3\,\mathrm{eV}$ below the Fermi level. (c) Sketch of the proposed band structure of the Schottky contact. (d) J–V curves of a typical Schottky solar cell prepared in this work in the dark and under illumination with simulated sunlight ($100\,\mathrm{mW/cm^2}$, simulated AM1.5G radiation). The solar cell represented here was prepared using 4 deposition cycles, a nanoparticle concentration of $40\,\mathrm{mg/mL}$, and an annealing temperature of $120\,^{\circ}\mathrm{C}$.

tron spectroscopy. Figure 3b shows a valence band spectrum of a $CuInS_2$ nanoparticle film on glass. The valence band maximum was found to be located about 0.3 eV below the Fermi level, meaning that the nanoparticles are p-type semiconductors. It should be noted that the nanoparticle sample studied by photoelectron spectroscopy was comparably prepared, but subjected to a surface treatment with hexanethiol. Thus, the samples used for solar cell preparation in this work, for the measurements by cyclic voltammetry and for the measurements by photoelectron spectroscopy had different ligand shells. On the other hand, another study of this material system has shown that at least the ligand exchange with

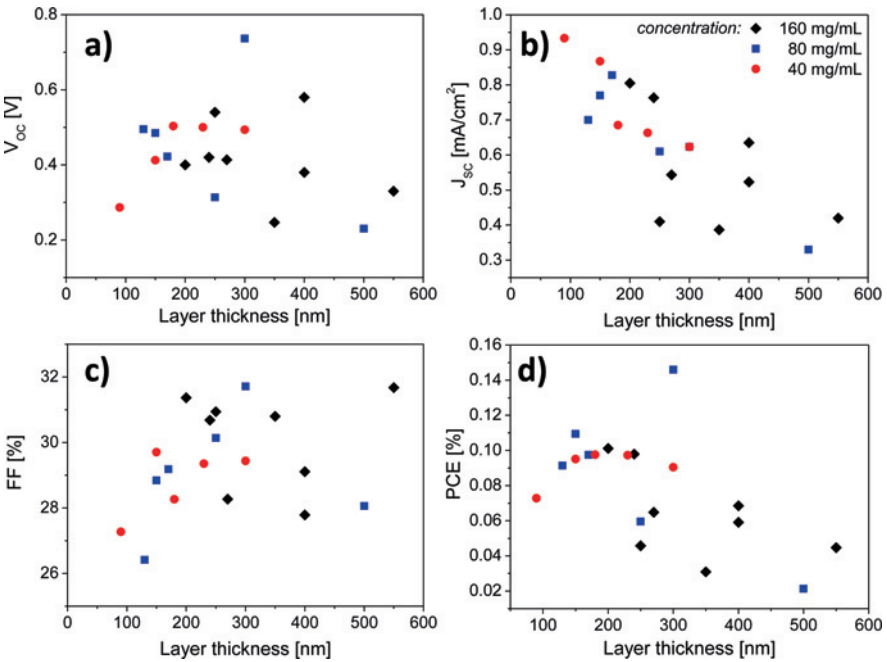

Figure 4: Results for the photovoltaic parameters of Schottky solar cells prepared with different numbers of layer-by-layer cycles and concentrations of the colloidal solutions used for spin-coating. The annealing temperature was 120 °C in all cases. The data is plotted against the thickness of the $CuInS_2$ nanoparticle layer (with the number of cycles not visible in this representation). Every data point represents an average over up to 8 individual solar cells prepared in the same configuration.

hexanethiol is by far not complete, but leaves a large fraction of the initial ligand shell unaffected [27]. Therefore, the differences with respect to the ligand shells are supposed to have only a minor influence on the results for the involved energy levels. Thus, we can tentatively propose the energy scheme sketched in Figure 3c for the Schottky solar cells realized in the present work. Different ligands as well as cross-linking molecules may have an influence on the exact position of the relevant energy levels, but a detailed analysis of these dependencies would go beyond the scope of this study.

Figure 3d shows typical J–V curves of the Schottky solar cells prepared within this study. This representative device had an open-circuit voltage (V_{OC}) of 0.50 V, a short-circuit current density (J_{SC}) of 0.65 mA/cm^2, a fill factor (FF) of 31% and a PCE of 0.10%. The $CuInS_2$ layer was prepared in 4 deposition cycles with the lowest nanoparticle concentration of 40 mg/mL, using 120 °C annealing temper-

ature, and had a thickness of about 230 nm. Obviously, the cells are basically working, but the performance is far behind that of Pb-based Schottky solar cells.

In order to investigate the impact of the absorber layer thickness, we performed systematic variations of the number of cycles and concentrations as preparation parameters, while using nanocrystals from the same synthesis batch. Figure 4 summarizes the results obtained for the photovoltaic parameters of the devices. The open-circuit voltage strongly scatters in the range between 0.25–0.75 V, without any systematic trends being obvious (Figure 4a). In contrast, a clear trend can be recognized for the photocurrent density (Figure 4b). Obviously, increasing the absorber layer thickness led to a reduction of the current density. This trend can be observed independently of the nanoparticle concentration used. Thereby, it is noteworthy that the data for the highest concentration scatter most strongly. This can be explained by the observation that the highest concentration enabled only poor control of the layer thickness by applying a defined number of deposition cycles (compare discussion above). The fill factor was rather constant for all cells and reached values between 28%–32% (Figure 4c). Only for very thin absorber layers (around 100 nm thickness), the fill factor was slightly lower. As a consequence of the dependencies mentioned, the power conversion efficiency roughly followed the trend of the photocurrent density in the sense that solar cells with the thickest absorber layers prepared had a reduced efficiency (Figure 4d). Within this work, many solar cells reached about 0.1% PCE, if the absorber layer thickness was in the range of approximately 150–250 nm.

The most interesting observation is the decrease of the photocurrent with increasing layer thickness. According to simple calculations based on the Beer-Lambert law, i. e., neglecting thin film interference effects, about 200 nm thickness of the $CuInS_2$ absorber layer should enable a maximum photocurrent density of about ~ 7.5 mA/cm^2 [20]. This is too low for highly efficient energy conversion. For comparison, PbSe-based Schottky solar cells with 4.6% power conversion efficiency were reported with the short-circuit current density amounting to about 17 mA/cm^2 [15]. Reaching comparable current densities with the $CuInS_2$ material would require layer thicknesses of the order of ~ 600 nm according to the simple calculations with the Beer-Lambert law [20]. Thus, from the point of view of efficient light absorption, the current density should be expected to significantly increase with the layer thickness in the range studied. In contrast, a decrease was experimentally observed. Moreover, at ~ 200 nm thickness, the photocurrent densities were about 10 times lower than the limit of 7.5 mA/cm^2 estimated by Beer-Lamberts' law. These findings provide a clear indication that loss mechanisms strongly restrict the extractable photocurrent. In more detail, the losses become more dominant with increasing layer thickness. This suggests that the losses are at least partly related to inefficient charge transport in the $CuInS_2$ layer.

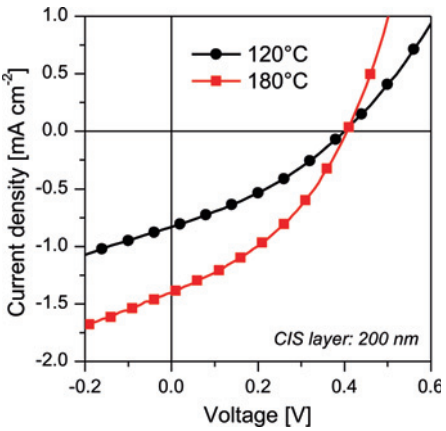

Figure 5: J–V curves under illumination with simulated sunlight of Schottky solar cells prepared with different annealing temperatures applied to the $CuInS_2$ layers. The absorber layer thickness was approximately 200 nm in both cases.

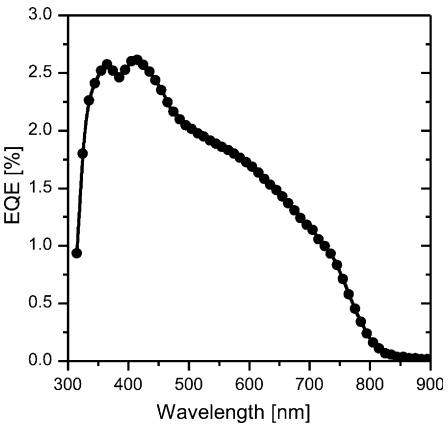

Figure 6: EQE spectrum of a Schottky solar cell prepared with an annealing temperature of 180 °C and an absorber layer thickness of 180 nm.

A parameter which might influence the charge transport characteristics is certainly the annealing procedure applied to the $CuInS_2$ layers in each deposition cycle. Therefore, we performed in the next step variations of the annealing temperature. Figure 5 shows J–V curves for representative devices with approximately 200 nm thick absorber layers which were annealed at 120 °C and 180 °C, respectively. Increasing the annealing temperature to 180 °C was found to have a beneficial effect on the short-circuit current density as well as the fill factor,

which reached 1.40 mA/cm^2 and 36.7%, respectively. Together with an open-circuit voltage of 0.41 V, a power conversion efficiency of 0.21% was obtained for the device represented in Figure 5. Nevertheless, the current density remained still about 5 times lower than the limit of 7.5 mA/cm^2 estimated above for a 200 nm thick absorber layer. Thus, annealing to higher temperature seems to reduce the transport limitation, but did not eliminate it. We also tried to increase the temperature further, but already with 220 °C, a strong reduction of the device performance was observed, mainly due to a strong drop of the open-circuit voltage. It is concluded that the devices do not support annealing at such high temperatures.

To investigate the spectral photoresponse, we measured also the external quantum efficiency of a few selected samples, and Figure 6 shows exemplarily the EQE spectrum of a device with a 180 nm thick absorber layer annealed at 180 °C. Significant generation of photocurrent starts at around ~ 800 nm and is extended over the whole visible range, the onset being in good agreement with the optical band gap of $CuInS_2$ nanoparticles [20, 26]. A few percent of quantum efficiency are reached in the maximum around ~ 400 nm.

4 Summary and conclusion

In the present work, colloidal quantum dot solids made of colloidal $CuInS_2$ nanocrystals were prepared by a layer-by-layer deposition technique using mercaptopropionic acid as cross-linker. Adjusting the concentration of the colloidal solutions as well as the number of deposition cycles enabled tuning the layer thickness in the range between 100–500 nm. However, lowering the concentrations and automating the process might be advisable in order to improve the degree of control in future.

The $CuInS_2$ layers were investigated with respect to their suitability as light absorber in Schottky solar cells. The devices showed a clear photoresponse, but the performance remained low compared to Schottky solar cells with Pb-based nanocrystals. Systematic investigations revealed the photocurrent density to decrease with increasing layer thickness, although light absorption should be improved. This strongly suggests charge transport to be a limiting factor in the devices. The annealing temperature was found to be a parameter which can improve the photocurrent. The best devices were obtained in this work at an annealing temperature of 180 °C and reached about 0.2% PCE under standard test conditions. Thereby, the short-circuit current densities still remained below the expectation deduced from the absorbance of the films.

Thus, the treatment with mercaptopropionic acid seems to be applicable to the $CuInS_2$ nanocrystals in order to enable layer-by-layer deposition, but charge transport in the obtained quantum dot solids appears to be limited in comparison to the established Pb-based systems. Possibly, mercaptopropionic acid does not replace enough of the initial ligands used in the synthesis of the $CuInS_2$ nanoparticles. Detailed studies of the charge transport characteristics as well as investigations of the ligand exchange in the films might bring progress to the future development of $CuInS_2$-based nanoparticle solar cells.

Acknowledgement: Funding from the "EWE-Nachwuchsgruppe Dünnschichtphotovoltaik" by the EWE AG, Oldenburg, is gratefully acknowledged.

References

1. H. Weller, Adv. Mater. **5** (1993) 88.
2. D. E. Gomez, M. Califano, and P. Mulvaney, Phys. Chem. Chem. Phys. **8** (2006) 4989.
3. J. Jasieniak, M. Califano, and S. E. Watkins, ACS Nano **5** (2011) 5888.
4. A. L. Rogach, N. Gaponik, J. M. Lupton, C. Bertoni, D. E. Gallardo, S. Dunn, N. L. Pira, M. Paderi, P. Repetto, S. G. Romanov, C. O'Dwyer, C. M. Sotomayor Torres, and A. Eychmüller, Angew. Chem. Int. Ed. **47** (2008) 6538.
5. D. V. Talapin, J.-S. Lee, M. V. Kovalenko, and E. V. Shevchenko, Chem. Rev. **110** (2010) 389.
6. H. Borchert: *Solar Cells Based on Colloidal Nanocrystals*, Springer Series in Materials Science, Volume 196, Springer-Verlag, Heidelberg (2014).
7. Y. Zhou, M. Eck, and M. Krüger, Energy Environ. Sci. **3** (2010) 1851.
8. H. Borchert, Energy Environ. Sci. **3** (2010) 1682.
9. T. Xu and Q. Qiao, Energy Environ. Sci. **4** (2011) 2700.
10. M. Wright and A. Uddin, Sol. Energy Mater. Sol. Cells **107** (2012) 87.
11. J. Y. Kim, O. Voznyy, D. Zhitomirsky, and E. H. Sargent, Adv. Mater. **25** (2013) 4986.
12. I. J. Kramer and E. H. Sargent, Chem. Rev. **114** (2014) 863.
13. R. Zhou, R. Stalder, D. Xie, W. Cao, Y. Zheng, Y. Yang, M. Plaisant, P. H. Holloway, K. S. Schanze, J. R. Reynolds, and J. Xue, ACS Nano **7** (2013) 4846.
14. Z. Liu, Y. Sun, J. Yuan, H. Wei, X. Huang, L. Han, W. Wang, H. Wang, and W. Ma, Adv. Mater. **25** (2013) 5772.
15. W. Ma, S. L. Swisher, T. Ewers, J. Engel, V. E. Ferry, H. A. Atwater, and A. P. Alivisatos, ACS Nano **5** (2011) 8140.
16. P. Maraghechi, A. J. Labelle, A. R. Kirmani, X. Lan, M. A. Adachi, S. M. Thon, S. Hoogland, A. Lee, Z. Ning, A. Fischer, A. Amassian, and E. H. Sargent, ACS Nano **7** (2013) 6111.
17. C.-H. M. Chuang, P. R. Brown, V. Bulović, and M. G. Bawendi, Nature Mater. **13** (2014) 796.
18. D. Aldakov, A. Lefrancois, and P. Reiss, J. Mater. Chem. C **1** (2013) 3756.
19. J. Kolny-Olesiak and H. Weller, ACS Appl. Mater. Interfaces **5** (2013) 12221.
20. D. Scheunemann, S. Wilken, J. Parisi, and H. Borchert, Appl. Phys. Lett. **103** (2013) 133902.

21. J. M. Luther, M. Law, M. C. Beard, Q. Song, M. O. Reese, R. J. Ellingson, and A. J. Nozik, Nano Lett. **8** (2008) 3488.
22. A. G. Pattantyus-Abraham, I. J. Kramer, A. R. Barkhouse, X. Wang, G. Konstantatos, R. Debnath, L. Levina, I. Raabe, M. K. Nazeeruddin, M. Grätzel, and E. H. Sargent, ACS Nano **4** (2010) 3374.
23. K. Szendrei, W. Gomulya, M. Yarema, W. Heiss, and M. A. Loi, Appl. Phys. Lett. **97** (2010) 203501.
24. J. Fritsche, A. Klein, and W. Jaegermann, Adv. Eng. Mater. **7** (2005) 914.
25. W. M. Haynes, D. R. Lide, and T. J. Bruno (Eds.), *CRC Handbook of Chemistry and Physics*, 94th edn., CRC Press, London (2013), p. 12–124.
26. N. Radychev, D. Scheunemann, M. Kruszynska, K. Frevert, R. Miranti, J. Kolny-Olesiak, H. Borchert, and J. Parisi, Org. Electron. **13** (2012) 3154.
27. C. Krause, R. Miranti, F. Witt, J. Neumann, D. Fenske, J. Paris, and H. Borchert, Sol. Energy Mater. Sol. Cells **124** (2014) 241.